VLBA Observations of Strong Anisotripic Radio Scattering Toward the Orion Nebula

Marina Kounkel[1] , Lee Hartmann[2] , Laurent Loinard[3,4] , Amy J. Mioduszewski[5], Luis F. Rodríguez[3] ,
Gisela N. Ortiz-León[6] , Michael D. Johnson[7] , Rosa M. Torres[8], and Cesar Briceño[9]

[1] Department of Physics and Astronomy, Western Washington University, 516 High Street, Bellingham, WA 98225, USA; Marina.Kounkel@wwu.edu
[2] Department of Astronomy, University of Michigan, 1085 S. University Street, Ann Arbor, MI 48109, USA
[3] Instituto de Radioastronomía y Astrofísica, Universidad Nacional Autónoma de México, Morelia 58089, Mexico
[4] Instituto de Astronomía, Universidad Nacional Autónoma de México, Apartado Postal 70-264, CdMx 04510, Mexico
[5] National Radio Astronomy Observatory, Domenici Science Operations Center, 1003 Lopezville Road, Socorro, NM 87801, USA
[6] Max Planck Institut für Radioastronomie, Auf dem Hügel 69, D-53121 Bonn, Germany
[7] Harvard-Smithsonian Center for Astrophysics, 60 Garden Street, Cambridge, MA 02138, USA
[8] Centro Universitario de Tonalá, Universidad de Guadalajara, Avenida Nuevo Periférico No. 555, Ejido San José, Tatepozco, C.P. 48525, Tonalá, Jalisco, México
[9] Cerro Tololo Interamerican Observatory, Casilla 603, La Serena, Chile

Abstract

We present observations of VLBA 20, a radio source found toward the edge of the Orion Nebula Cluster (ONC). Nonthermal emission dominates the spectral energy distribution of this object from the radio to mid-infrared regime, suggesting that VLBA 20 is extragalactic. This source is heavily scattered in the radio regime. Very Long Baseline Array observations resolve it to $\sim 34 \times 19$ mas at 5 GHz, and the wavelength dependence of the scattering disk is consistent with ν^{-2} at other frequencies. The origin of the scattering is most likely the ionized X-ray emitting gas from the winds of the most massive stars of the ONC. The scattering is highly anisotropic, with the axis ratio of 2:1, higher than what is typically observed toward other sources.

Key words: HII regions – ISM: magnetic fields – scattering

1. Introduction

Interstellar scattering of extragalactic sources in the radio regime is a phenomenon caused by turbulent ionized gas located along the line of sight. It has been observed in a number of sources located behind Galactic H II regions and typically affects sub-GHz frequencies observations; comparatively, few sources are known in which scattering is observed at frequencies above a few GHz. The strongest known scatter broadening is found toward NGC 6334B, where the scattering disk has a size of 300 mas at 5 GHz (Trotter et al. 1998). Other regions with strongly scattered sources include the galactic center (e.g., Backer 1978; Bower & Backer 1998; Ortiz-León et al. 2016), the Cygnus regions (e.g., Wilkinson et al. 1994; Desai & Fey 2001), B1849+005 (Lazio 2004), and possibly M17 (Rodríguez et al. 2014). Recently, Kounkel et al. (2017) have also identified a region of scattering associated with the ionized gas region produced by a supernova in the λ Ori cluster toward several sources, most strongly toward J0536+0944. In most of these cases, the scattering disk appears to be somewhat anisotropic, with the typical axial ratio of 1.2–1.5. This anisotropy is thought to be associated with the magnetic activity within the H II regions, with the preferential direction of the scattering aligned perpendicularly to the magnetic fields (Narayan et al. 1989).

In the process of mapping the Orion Molecular Cloud Complex with the Very Long Baseline Array (VLBA), Kounkel et al. (2017) have identified a peculiar source, VLBA 20 (Figure 1), which is located toward the west of the Orion Nebula Cluster (ONC). This source appeared to be resolved, and highly anisotropic, with a size of 34×19 mas at 5 GHz. No coherent emission was apparent at baselines beyond 8 Mλ. Five epochs were observed in total, and the morphology was largely consistent in all of them. In this paper, we examine the nature of VLBA 20 and the origin of its morphology.

2. Multi-wavelength Observations

VLBA 20 (=GBS-VLA J053424.63-052838.5) was first identified in the Very Large Array (VLA) survey of the ONC (Kounkel et al. 2014). It was observed as a point source at 4.5 and 7.5 GHz, with fluxes of $F_{4.5\,\mathrm{GHz}} = 47.31 \pm 2.37$ mJy and $F_{7.5\,\mathrm{GHz}} = 32.95 \pm 1.66$ mJy. Three different epochs have been obtained over a period of two months; no variability in flux was observed. Aside from Kounkel et al. (2014) and Kounkel et al. (2017), no fluxes for VLBA 20 have been published. This source was originally identified as a young stellar object candidate; however, subsequent astrometric observations with VLBA have ruled out this interpretation due to a lack of any parallax or proper motions. In order to confirm that the detected radio emission is nonthermal as well as to determine the true nature of this source, we examined the archival data to construct its spectral energy distribution. When possible, we also analyzed the variability of the source.

While not previously reported, a number of radio detections of VLBA 20 exist. Yusef-Zadeh has observed it with the VLA in four different configurations at 4.8 GHz between 1988 and 1989 (project code: AY24). We reduced and imaged all of the archival data following the standard prescription in AIPS. The measured flux was $F_{4.8\,\mathrm{GHz}} = 48 \pm 1$ mJy in all four epochs, consistent with our recent observations, showing no variability over a 25 year baseline. Additionally, it has been detected at 1.4 GHz in 1984 (Dulk, project code AD114) and 1987 (Yusef-Zadeh, project code AC170) with flux of $F_{1.4\,\mathrm{GHz}} = 106 \pm 1$ mJy. In all of the VLA observations, this source appears point-like.

Only hints of the detection are available in any wavelength regimes other than radio (Table 1). VLBA 20 has been previously detected with the *Hubble Space Telescope* (*HST*) at 0.775 and 0.85 μm (Da Rio et al. 2009) and with the *Spitzer* Space Telescope at 3.6 and 4.5 μm (Morales-Calderón et al. 2011) during optical and infrared surveys of the Orion
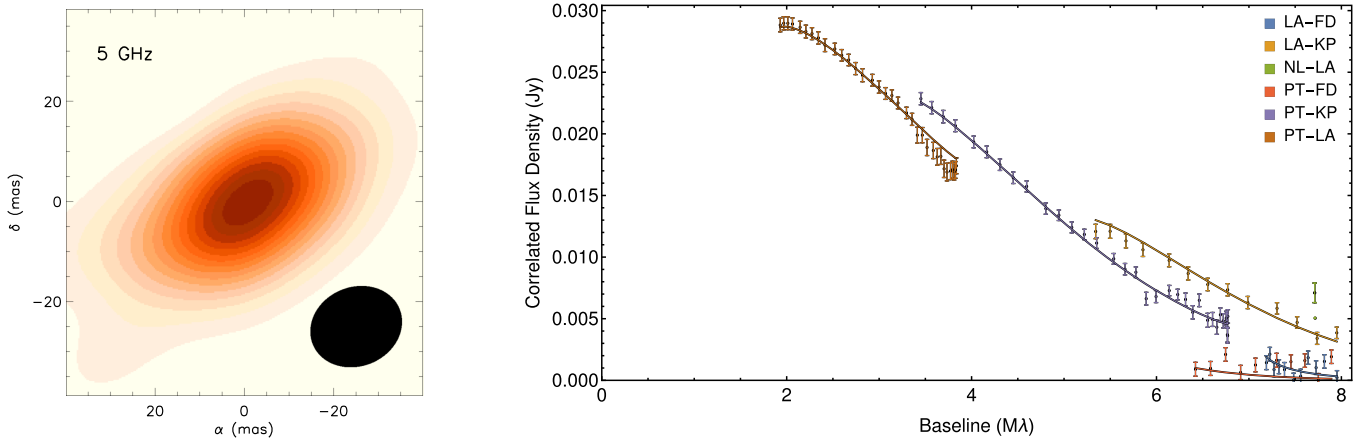
Figure 1. VLBA 20, as seen at 5 GHz with VLBA, with data combined from five epochs observed. Left panel: imaging of the source, with the UV range limited to 8 Mλ, as no coherent emission is apparent beyond it. The corresponding synthesized beam is shown in black. Right panel: visibility amplitude as a function of UV distance.

Table 1
Fluxes of Multi-wavelength Observations of VLBA 20

ν	F
1.4 GHz	106 ± 1 mJy
4.5 GHz	47.31 ± 2.37 mJy
7.5 GHz	32.95 ± 1.66 mJy
224.521 GHz	2 ± 1 mJy
336.425 GHz	<1 mJy
4.5 μm	16.49 ± 0.14 mag
3.6 μm	17.11 ± 0.11 mag
2.2 μm	>22 mag
1.6 μm	>20.9 mag
1.25 μm	>21.5 mag
1.03 μm	>22.1 mag
0.85 μm	~ 24 mag
0.775 μm	~ 27 mag
5 keV	$<6 \times 10^{-15}$ erg s^{-1} cm^{-2}

Figure 2. Spectral energy distribution of VLBA 20, combining observations from VLA, VLBA, SMA, *Spitzer*, and *HST*.

region. Unfortunately, due to the faintness of the source and insufficiently deep exposures, the *HST* detections are only barely significant and it is impossible to obtain reliable photometry. We estimate $m_{0.775\,\mu m} \sim 27$, $m_{0.85\,\mu m} \sim 25$. *Spitzer* data yielded $m_{3.6\,\mu m} = 17.11 \pm 0.11$, $m_{4.5\,\mu m} = 16.49 \pm 0.14$. No sufficiently deep *J, H,* and *K* band exposures exist, but we estimate $m_Y > 22.1$, $m_J > 21.5$, $m_H > 20.9$ based on the sensitivity of the Galactic Cluster Survey performed as part of the United Kingdom Infrared Telescope (UKIRT) Infrared Deep Sky Survey, $m_K > 22$ based on the National Optical Astronomy Observatory Extremely Wide-field Infrared Imager (NEWFIRM) observations toward that region (S. T. Megeath et al. 2018, in preparation), as well as $m_{5.8\,\mu m} > 14$ and $m_{8\,\mu m} > 13$ from the *Spitzer* survey (Megeath et al. 2012). *Chandra* observations yielded a 95% confidence upper limit of 6×10^{-15} erg s^{-1} cm^{-2} (Audard et al. 2005).

We observed VLBA 20 with the Submillimeter Array (SMA) on 2015 December 13 in the compact configuration at two frequencies (224.521 and 336.425 GHz) with an integration time of 400 minutes. Uranus and Callisto were used for flux calibration, 3C454.3 was used as the bandpass calibrator, and 0501-019 and 0607-085 were used as the gain calibrators. The data were reduced and calibrated following the standard prescriptions using the IDL package MIR as well as MIRIAD
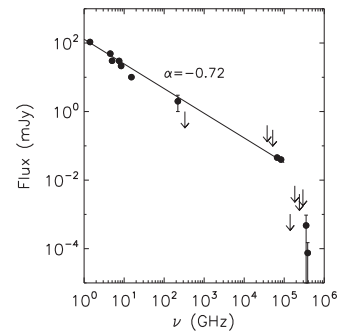
(Sault et al. 1995). A weak detection was obtained at 224.521 GHz with a measured flux of 2 ± 1 mJy. VLBA 20 was not detected at 336.425 GHz, with a 1σ noise limit of 1 mJy. No molecular lines have been detected within the bandwidth of 4 GHz at either wavelength.

The radio to near-infrared flux of VLBA 20 can be fitted by a power law with a slope of $\alpha = -0.72$, defined such that $S_\nu \propto \nu^\alpha$ (Figure 2). The spectrum is consistent with an AGN-related activity (e.g., Carilli et al. 1999) and provides a clear indication that the radio emission has little or no thermal component.

3. Multi-frequency VLBI Observations

In order to constrain the morphology of VLBA 20 and to complement existing 5 GHz observations from Kounkel et al. (2017), we obtained VLBA observations at 8.4 and 15.2 GHz. On both cases, the bandwidth was 256 MHz (8.304–8.528 and 15.144–15.368 GHz, respectively). The observations took place on 2017 July 1 and 2, with the total observing time of 8 hr shared between these dates. J0501-0159 was used to correct for the instrumental delays and J0529-0519 was used as the primary calibrator to estimate and remove residual rates, delays, and phases. The observing strategy was to alternate between 150 s on source and 50 s on the primary calibrator for a combined total time of 152 minutes on source at 8.4 GHz for the two dates, and 120 s on source and 50 s on the primary calibrator for a combined total of 182 minutes on source at 15.2 GHz. The data were reduced in AIPS (Greisen 2003); the
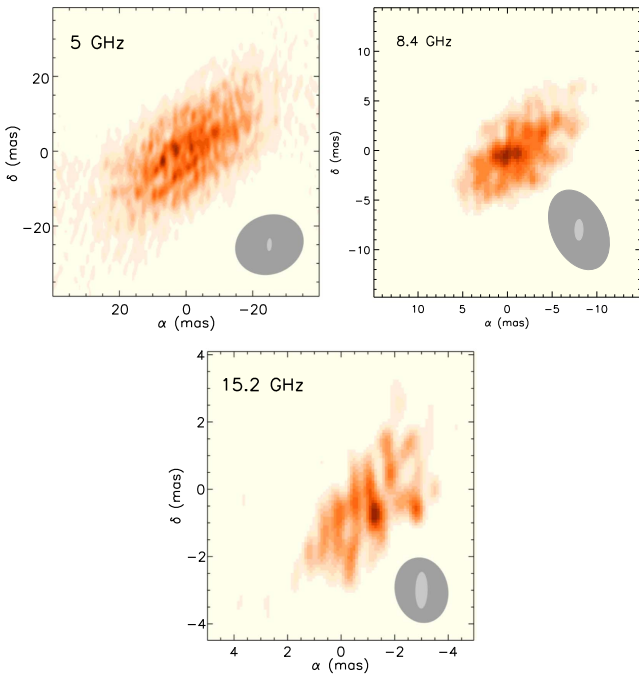
Figure 3. VLBA 20 imaged at 5 GHz, 8.4 GHz, and 15.2 GHz, with the full UV range. Due to a lack of coherent signal at large baselines, imaging does not perfectly recover the smooth profile of the scattering disk, producing a stippling effect. Imaging is done using uniform weighting; other schemes do not substantially improve the image. Note that the size of the panel is different at each wavelength. Two beam sizes are shown, the beam corresponding to the full UV range (light gray), and the beam produced by limiting the UV range to the baselines with the coherent signal (dark gray).

full description of data processing is presented in Ortiz-León et al. (2017) and Kounkel et al. (2017).

The morphology observed at 5 GHz persists at the other wavelengths as well (Figure 3). We report on the dimensions of the source, which were obtained in the UV plane, by fitting a Gaussian profile using the CASA task uvmodelfit, in Table 2. The dimensions are consistent with what is obtained in the image plane. At 8.4 GHz, no coherent signal was apparent beyond 23 Mλ. Similarly, at 15.2 GHz, no coherent signal originated from beyond 45 Mλ. The wavelength dependence in both the major and the minor axes of the scattering disk can be fitted by a power law with a slope α of -1.75 ± 0.02 and -1.98 ± 0.06, respectively (Figure 4). For the minor axis, the relationship is consistent with $\alpha = -2$, which is the expected wavelength dependence for interstellar scattering. The major axis does deviate from this somewhat, but it is still largely consistent. It is possible that the deviation from the expected slope may be significant, although data at a larger number of frequencies would be required to more conclusively determine it. It may also be notable that both the semimajor and the semiminor axes at 15.2 GHz appear to be slightly above the fit, and it is possible that at these high frequencies, we may be starting to detect the intrinsic dimensions of the source.

It should be noted that at all of the frequencies, the gain calibrator J0529-0519 does not appear to be resolved. In all of observations, its deconvolved components are generally consistent with a true point source. A strong signal is present in all of the baselines. The same can be said of the secondary calibrators used in Kounkel et al. (2017), although J0539-0514, while also unresolved, does have its signal taper off on the longest baselines involving the Mauna Kea (MK) VLBA

station in Hawaii. Other confirmed extragalactic sources toward the ONC might be weakly affected by scattering,[10] with the nominal deconvolved dimensions of up to 1–2 mas at 5 GHz, but none as extreme as VLBA 20.

The origin of the scattering is most likely to be the hot X-ray emitting gas produced by the high-velocity winds from θ^1 Ori C, which was previously observed by Güdel et al. (2008). It is notable that very few extragalactic radio sources appear to be observed toward this gas[11] (Figure 5), although a number are found near the outer bounds. In comparison to the other regions targeted by the VLA survey, a number of extragalactic sources near the H II region in the ONC may be underestimated by a factor of 1.5–2, although it is not clear what is responsible for it.

In general, the angular size θ_{scatt} of a scattered point source depends both on the diffractive scale (r_{diff}) of the scintillation and on the relative scattering geometry. Physically, the diffractive scale corresponds to the transverse length on the phase screen over which the random phase introduced by scattering shows a root-mean-squared difference of 1 radian. Thus, it quantifies the strength of the phase fluctuations of scattering. Specifically (see, e.g., Taylor & Cordes 1993; Trotter et al. 1998)

$$\theta_{scatt} \approx \frac{\sqrt{2 \ln 2}}{\pi} \frac{\lambda}{(1 + M) r_{diff}} \approx 0.37 \frac{\lambda}{(1 + M) r_{diff}}$$

where M is the "magnification" of the scattering, equal to the observer-scattering distance divided by the source-scattering distance.

In the special case of an extragalactic source, $M \approx 0$. In this case, the angular broadening is independent of the distance from the observer to the scattering material: $\theta_{scatt} \approx 0.37 \frac{\lambda}{r_{diff}}$. Note that θ_{scatt} scales approximately as λ^2, and r_{diff} scales approximately as $1/\lambda$.

For VLBA 20, we find $\theta \approx 34$ mas for the major axis at 5 GHz, giving $r_{diff} \approx 130$ km at that frequency. In contrast, typical angular broadening off the Galactic plane is ~ 1 mas$/\nu^2_{GHz}$, giving $r_{diff} \sim 10^5$ km at 5 GHz (Cordes & Lazio 2002). Thus, the absolute density fluctuations along the line of sight to VLBA 20 (integrated through the scattering material) are stronger by a factor of ~ 1000 than the "typical" values, although it is comparable in strength to the other regions that are associated with strong scattering.

It is notable that the effect of interstellar scattering toward VLBA 20 is highly anisotropic in nature, with the axis ratio being consistent with 2:1 in all observations. Frequently, a higher axis ratio is apparent toward pulsars at frequencies less than 1 GHz (e.g., Rickett 2006). A comparable degree of anisotropy has been seen toward Sgr A* at 8.7 GHz, although the axis ratio appears to significantly decrease at 15.4 GHz and higher frequency data (Bower et al. 2014; Ortiz-León

---

[10] On the other hand, members of the ONC are largely unaffected by angular broadening. Most of the photons would be scattered too strongly to converge at the position of the observer due to a wider range of the angles that reach the scattering screen, and, similarly to the other lensing-like effects, the remaining ones would not disperse over a sufficiently large solid angle to create as strongly scatter broadened image as a more distant source would be able to produce.

[11] Another source is projected onto the diffuse X-ray emission, GBS-VLA J053418.01-054255.4. This source was not observed with the VLBA. It is not clear whether interstellar scattering would affect it or not as the X-ray emission toward it is patchy. In VLA observations it was point-like and comparatively faint ($F_{4.5 \, GHz} = 0.34$ mJy).

Table 2
Deconvolved Gaussian Model of VLBA 20

ν[a] (GHz)	S (mJy)	a (mas)	b (mas)	p.a. (deg)	q
5[a]	34.0 ± 0.14	34.4 ± 0.6	19.4 ± 0.7	125.3 ± 0.5	0.56 ± 0.01
8.4	24.5 ± 0.16	12.4 ± 0.1	6.5 ± 0.1	129.2 ± 0.4	0.52 ± 0.01
15.2	10.0 ± 0.2	5.0 ± 0.1	2.3 ± 0.3	138.8 ± 1.8	0.45 ± 0.02

Note.
[a] Multiple epochs are concatenated.
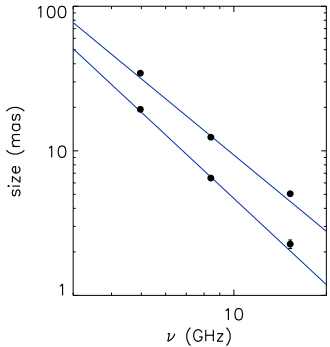
Figure 4. Wavelength dependence of the semimajor and semiminor axes of VLBA 20, with the respective fitted slopes of -1.75 ± 0.02 and -1.98 ± 0.06.

Figure 6. Map of magnetic field lines toward the Orion from *Planck* (Planck Collaboration et al. 2016), with the approximate position and orientation of VLBA 20.

Figure 5. Spitzer map of the ONC with the superimposed diffuse X-ray emission (in blue) from Güdel et al. (2008). The dots are the observed radio sources with VLA from Kounkel et al. (2014). Blue dots represent known members of the ONC. White dots represent that membership status is unknown or likely extragalactic. The red dot represents VLBA 20.

et al. 2016). VLBA 20 appears to have a scattering disk with a highest axis ratio at frequencies of 15.2 GHz, and possibly higher. If 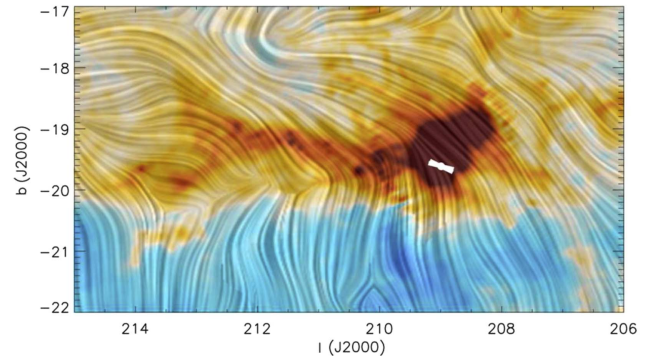magnetic fields are an explanation for this anisotropy in this case, it suggests that they may be more coherent toward VLBA 20 than in the other H II regions associated with interstellar scattering. While the position angle does appear to slightly rotate with wavelength, the orientation of VLBA 20 is broadly consistent with being perpendicular to the magnetic field lines mapped by *Planck*, even though it does appear to deviate from it somewhat (Planck Collaboration et al. 2016). We note, however, that owing to the low angular resolution of the *Planck* data, it is difficult to make a more precise comparison, and higher-resolution mapping of the magnetic fields is necessary to confirm it one way or another (Figure 6).

At all frequencies, the emission toward VLBA 20 does not have a smooth profile; rather, the scattering disk deconvolves into a series of stipples with the size comparable to the size of a beam (Figure 3). Efforts have been made to understand whether this may be attributed to speckles, such as if the substructure is produced by the refractive noise that is present on long baselines (Johnson & Gwinn 2015). This has been found to be unlikely. Most probably, the stippling effect can be attributed to an imperfect reconstruction of a Gaussian profile while imaging due to the noise from the non-detection of the signal on long baselines. Removing those baselines does produce a smoother image (e.g., Figure 1). At higher frequencies, the size of the degraded beam becomes comparable to the size of the source. Nonetheless, the anisotropy and the true dimensions of the source can be recovered during deconvolution even in the degraded images.

4. Conclusions

We present VLBA observations of a peculiar radio source, VLBA 20. This source is projected near the ONC, but it is extragalactic, with nonthermal emission dominating the spectrum down to infrared wavelengths. VLBA 20 is heavily

scattered by the H II region produced by the most massive stars of the ONC. The degree of scattering is comparable to what has been previously observed toward Cyg X3 (Wilkinson et al. 1994) and Sgr A* (Bower et al. 2014), although it is weaker than that toward NGC 6334B (Trotter et al. 1998). This source is highly anisotropic, with the scattering disk resolved to $\sim 34 \times 19$ mas at 5 GHz. Higher frequency observations preserve the axis ratio, scaling the size by $\sim \nu^{-2}$. This anisotropy is most likely driven by the strong magnetic fields within the turbulent plasma.

Software: AIPS (Greisen 2003), MIRIAD (Sault et al. 1995), MIR (https://www.cfa.harvard.edu/~cqi/mircook.html).

ORCID iDs

Marina Kounkel ● https://orcid.org/0000-0002-5365-1267
Lee Hartmann ● https://orcid.org/0000-0003-1430-8519
Laurent Loinard ● https://orcid.org/0000-0002-5635-3345
Luis F. Rodríguez ● https://orcid.org/0000-0003-2737-5681
Gisela N. Ortiz-León ● https://orcid.org/0000-0002-2863-676X
Michael D. Johnson ● https://orcid.org/0000-0002-4120-3029

References

Audard, M., Güdel, M., Skinner, S. L., et al. 2005, ApJL, 635, L81
Backer, D. C. 1978, ApJL, 222, L9
Bower, G. C., & Backer, D. C. 1998, ApJL, 496, L97
Bower, G. C., Deller, A., Demorest, P., et al. 2014, ApJL, 780, L2
Carilli, C. L., Kurk, J. D., van der Werf, P. P., Perley, R. A., & Miley, G. K. 1999, AJ, 118, 2581
Cordes, J. M., & Lazio, T. J. W. 2002, arXiv:astro-ph/0207156
Da Rio, N., Robberto, M., Soderblom, D. R., et al. 2009, ApJS, 183, 261
Deller, A. T., Brisken, W. F., Phillips, C. J., et al. 2011, PASP, 123, 275
Desai, K. M., & Fey, A. L. 2001, ApJS, 133, 395
Greisen, E. W. 2003, Astrophysics and Space Science Library, Vol. 285, Information Handling in Astronomy—Historical Vistas (Dordrecht: Kluwer), 109
Güdel, M., Briggs, K. R., Montmerle, T., et al. 2008, Sci, 319, 309
Johnson, M. D., & Gwinn, C. R. 2015, ApJ, 805, 180
Kounkel, M., Hartmann, L., Loinard, L., et al. 2014, ApJ, 790, 49
Kounkel, M., Hartmann, L., Loinard, L., et al. 2017, ApJ, 834, 142
Lazio, T. J. W. 2004, ApJ, 613, 1023
Megeath, S. T., Gutermuth, R., Muzerolle, J., et al. 2012, AJ, 144, 192
Morales-Calderón, M., Stauffer, J. R., Hillenbrand, L. A., et al. 2011, ApJ, 733, 50
Narayan, R., Anantharamaiah, K. R., & Cornwell, T. J. 1989, MNRAS, 241, 403
Ortiz-León, G. N., Johnson, M. D., Doeleman, S. S., et al. 2016, ApJ, 824, 40
Ortiz-León, G. N., Loinard, L., Kounkel, M. A., et al. 2017, ApJ, 834, 141
Planck Collaboration, Ade, P. A. R., Aghanim, N., et al. 2016, A&A, 586, A138
Rickett, B. 2006, ChJAS, 6, 197
Rickett, B. J. 1990, ARA&A, 28, 561
Rodríguez, L. F., Carrasco-González, C., Montes, G., & Tapia, M. 2014, AJ, 148, 20
Sault, R. J., Teuben, P. J., & Wright, M. C. H. 1995, in ASP Conf. Ser. 77, Astronomical Data Analysis Software and Systems IV, ed. R. A. Shaw, H. E. Payne, & J. J. E. Hayes (San Francisco, CA: ASP), 433
Taylor, J. H., & Cordes, J. M. 1993, ApJ, 411, 674
Trotter, A. S., Moran, J. M., & Rodríguez, L. F. 1998, ApJ, 493, 666
Wilkinson, P. N., Narayan, R., & Spencer, R. E. 1994, MNRAS, 269, 67